Solubility, Speciation and Thermodynamics of $PuCO_3OH(cr)$ in Carbonate Containing NaCl Solutions

Philipp Müller, David Fellhauer,* Dieter Schild, Xavier Gaona, Kathy Dardenne, Jörg Rothe, Marcus Altmaier, and Horst Geckeis*

Abstract: The solubility, aqueous speciation, and solid phase formation of trivalent plutonium, Pu(III) was investigated for the first time in pH near-neutral 0.10 M NaCl solutions under the presence of carbonate at $T = (23 \pm 2)$ °C in the frame of a comprehensive experimental study. Crystalline $PuCO_3OH(cr)$ was synthesized by long-term equilibration of the binary hydroxide $Pu(OH)_3(am)$ in aqueous Na_2CO_3 solutions and comprehensively characterized by VIS/NIR absorption spectroscopy, SEM/EDX, powder XRD and Rietveld analysis, and Pu L3-edge EXAFS. Batch solubility experiments with $PuCO_3OH(cr)$ equilibrated in 0.10 M NaCl–Na_2CO_3 solutions were performed from undersaturation as a function of pH_m and followed over time for up to 90 days. A chemical model was derived and the corresponding thermodynamic constants evaluated. These novel data demonstrate that under specific conditions Pu(III) equilibrium concentrations are up to three orders of magnitude lower when controlled by the $PuCO_3OH(cr)$ compared to the concentration level defined by $Pu(OH)_3(am)$, and reveal a remarkable stabilization of the entire Pu(III) oxidation state in carbonate containing aqueous solutions. The relevance of the new data for geochemical modeling of environmental systems and nuclear waste repositories is discussed.

Introduction

The aqueous chemistry of early actinides (Th–Cm) provides important insights into their reactivity and interactions in aquatic systems relevant to nuclear engineering, waste disposal, and environmental chemistry. Today, the context of many applied studies on actinides is related to assess their environmental and geochemical properties.[1] This concerns on one hand the already existing large-scale distributions of transuranium elements in the environment at trace levels due to nuclear weapon tests and releases from nuclear (legacy) sites. On the other hand, being the focus of the present study, the potential radionuclide release from nuclear waste repositories on future timescales is of great interest. Investigations into repository science also address one of the challenges of the nuclear fuel cycle. The direct disposal in deep geological formations is the internationally favored option for the safe long-term storage of nuclear waste.[2,3] Initially emplaced as materials immobilized in solid structures, namely by placing fuel assemblies and vitrified waste in specific steel casks, potentially contacting aqueous solutions, e.g. inflowing groundwater, may lead to corrosion of the waste matrixes and subsequent release of radionuclides. Migration of the latter into the biosphere pose a radiological risk on long-time scales, which is evaluated as part of the Safety Case for nuclear waste repositories.[2,4,5] Studies on the aqueous chemistry and thermodynamics of radionuclides are relevant in this context and provide the required input parameters (chemical models, equilibrium constants, activity coefficients) to reliably predict geochemical reactions like solubility equilibria, complexation, redox reactions, sorption, and incorporation into mineral phases, etc., and their respective dependence on relevant solution parameters, e.g., pH, redox potential, ionic strength, etc.

Plutonium is the main transuranic element in spent nuclear fuel.[6,7] Notorious for its pronounced redox sensitivity, Pu can be present in aqueous solution particularly in the oxidation states + III to + VI.[8–11] Under the strongly reducing conditions expected for operative repositories in deep geological formations,[1,12,13] Pu(III) and Pu(IV) are the predominant oxidation states.[9] In the absence of other ligand systems, equilibrium reactions between the (hydr)oxide phases $Pu(OH)_3(am)$ or $PuO_2(s, hyd)$, and dissolved hydrolysis complexes $Pu(OH)_x^{3-x}$ with $x = 0$–3 and $Pu(OH)_y^{4-y}$ with $y = 0$–4, control the solubility of Pu(III) and Pu(IV) (Figure S1), respectively. $PuO_2(s, hyd)$ is the least soluble binary Pu-oxyhydroxo phase of all Pu oxidation states, and limits dissolved Pu(IV) to, e.g., $\log [Pu(IV)] \approx -10.5$ at pH ≥ 7. The solubility of $Pu(OH)_3(am)$ is about six orders of magnitude greater at pH 7, but approaches the low solubility level of $PuO_2(s, hyd)$ at high alkalinity with $pH_m \geq \approx 11$.[14] The excerpt of the Pu Pourbaix diagram displayed in Figure 9 is based on the data of the thermochemical database project of the OECD (Organization for Economic Co-operation and Development)–Nuclear Energy Agency (NEA-TDB[15]). It highlights the stability fields of the different Pu species and

[*] P. Müller, D. Fellhauer, D. Schild, X. Gaona, K. Dardenne, J. Rothe, M. Altmaier, H. Geckeis
Institute for Nuclear Waste Disposal, Karlsruhe Institute of Technology 76021, Karlsruhe, Germany
E-mail: philipp.mueller2@kit.edu
david.fellhauer@kit.edu

oxidation states as a function of pH and the redox potential pe (with pe = 16.9·E_h at T = 298.15 K).[14,16] The position of the Pu(III)–Pu(IV) transition borderline calculated for [Pu_{tot}] = 2 mM (grey dashed line) is only slightly above the lower decomposition line of water at pe+pH = 0,[17] revealing that Pu(III) is only stable under strongly reducing conditions whereas Pu(IV) is the predominant Pu oxidation state over a wide ranges of pe and pH conditions. The corresponding diagram showing the stability fields in absence of solid Pu phases is provided in the Figure S1.

Carbonate is ubiquitous in environmental systems and known to strongly interact with actinides in all their oxidation states.[18,19] The carbonate influence on the solubility, speciation, and solid phase formation of radionuclides can be important in geochemically based long-term safety assessments for nuclear waste repositories. The impact of carbonate on solubility equilibria of Pu(IV) was investigated in several studies,[20–25] revealing that binary $Pu(CO_3)_x^{4-2x}$ aqueous species with x = 4–5 can form particularly at high pCO_2 whereas mixed $Pu(OH)_x(CO_3)_y^{4-x-2y}$ are relevant for low to intermediate pCO_2 and in solubility controlled systems. To the best of our knowledge, there are no systematic studies on the solubility behavior of Pu(III) in the presence of carbonate. Carbonate was found to have a major influence on the solubility and speciation of the chemical analogs Am(III) and Ln(III) due to the formation of carbonate containing complexes $(An(III)(CO_3)_n^{3-2n})$[26–28] and solid phases like $AnCO_3OH(cr)$, $An_2(CO_3)_3{\cdot}xH_2O(s)$, $NaAn(CO_3)_2{\cdot}xH_2O(s)$ and $Na_3An(CO_3)_3{\cdot}xH_2O(s)$.[26–29] In pH near-neutral carbonate containing NaCl solutions, $AmCO_3OH(cr)$ is considerably more stable and hence less soluble than the corresponding hydroxide phase, $Am(OH)_3(am)$.[7,28,30] A comparable stabilization likely exists for Pu(III), significantly impacting the Pu(III)–Pu(IV) redox borderline, but this has not been demonstrated yet based on experimental evidence. While the hydrothermal synthesis and characterization of $PuCO_3OH(cr)$ was reported previously,[31] no experimental study was dedicated to its solubility, speciation, and thermodynamics in aqueous solutions at room temperature.

In the present work, we report the synthesis, characterization and first comprehensive solubility study on $PuCO_3OH(cr)$ in carbonate containing 0.10 M NaCl solutions and reveal its significant impact on aqueous Pu systems under reducing conditions.

Results

Pu Solid Phase Characterization

Figure 1 shows the VIS/NIR spectrum of the Pu(III) transformation product, $PuCO_3OH(cr)$, digested in 0.5 M $HClO_4$ (black) and measured directly after digestion in comparison to the reference spectrum of $Pu^{3+}(aq)$ in 1 M $HClO_4$ (red) reported by Cohen.[32] The excellent agreement of both spectra confirms that the transformation product is a pure Pu(III) compound. No indications for other Pu oxidation states were detected in the spectrum.

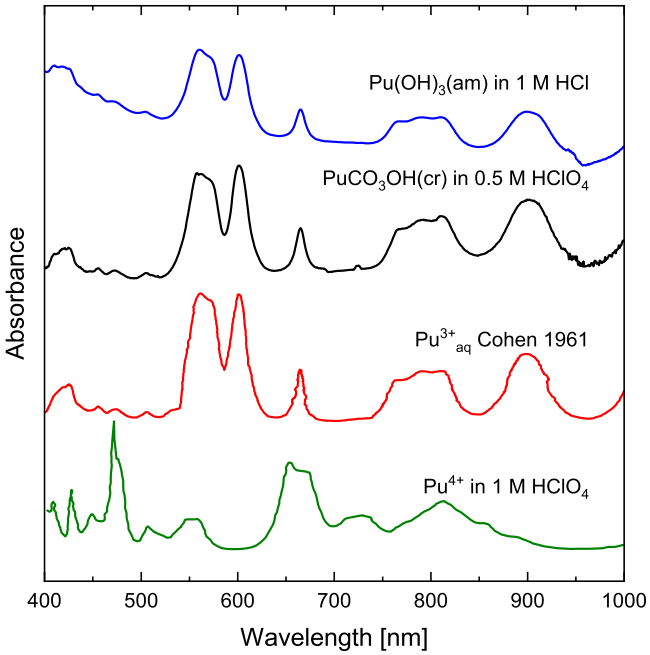


Figure 1. VIS/NIR spectra of $Pu(OH)_3(am)$ digested in 1 M HCl (blue), $PuCO_3OH(cr)$ digested in 0.5 M $HClO_4$ (black), $Pu^{3+}(aq)$ in 1 M $HClO_4$ reference reported by Cohen (red)[32] and Pu^{4+} in 1 M $HClO_4$ (green).[14]

Table 1: Elemental EDX composition [Atom%] and C : Pu : O ratio of $PuCO_3OH(cr)$. Average value includes EDX results from the first and the second synthesis (reproduction) listed in the (Table S1).

SEM	Pu [Atom%]	C [Atom%]	O [Atom%]	EDX Pu : C : O
Figure 2b	18.4 (± 0.6)	18.2 (± 0.5)	58.1 (± 1.4)	1.0 : 0.9 : 3.2
Figure 2c	18.2 (± 0.6)	16.2 (± 0.4)	61.4 (± 1.4)	1.0 : 0.9 : 3.4
Figure 2d	19.9 (± 0.7)	17.6 (± 0.5)	58.3 (± 1.4)	1.0 : 0.9 : 2.9
Figure 2e	19.7 (± 1.0)	17.2 (± 0.7)	59.0 (± 2.1)	1.0 : 0.9 : 3.0
Average	19.5 (± 0.8)	20.0 (± 0.6)	54.8 (± 1.7)	1.0 : 1.0 : 2.8

The SEM images displayed in Figure 2 reveal that the transformation product in both syntheses, $PuCO_3OH(cr)$, was obtained as a homogeneous material. The first synthesis yielded crystals varying in size from 20–100 µm (Figure 2a). Figure 2b,c highlights that the individual crystals are agglomerates of small (lamellar) platelets. The morphology of $PuCO_3OH(cr)$ differs significantly from the amorphous precursor $Pu(OH)_3(am)$ which consists of ill-defined agglomerated particles with very small particle size (≈few nm), see Figure S2. $PuCO_3OH(cr)$ obtained in the second synthesis showed diminished crystallinity, with crystallites sizes ranging from 1–5 µm (Figure 2d). Figure 2e reveals that the shape of the individual crystallites still resembles the lamellar platelets observed in the first synthesis. Exchanging the matrix solution twice in the second synthesis appears to promote the formation of smaller crystals. Table 1 shows the elemental composition by SEM-EDX of the crystals depicted in Figure 2b–e as well as the average composition. The C : Pu : O ratios are close to the formal composition of $PuCO_3OH(cr)$.

Figure 3 shows the powder diffraction patterns of the starting material, $Pu(OH)_3(am)$, and the transformation

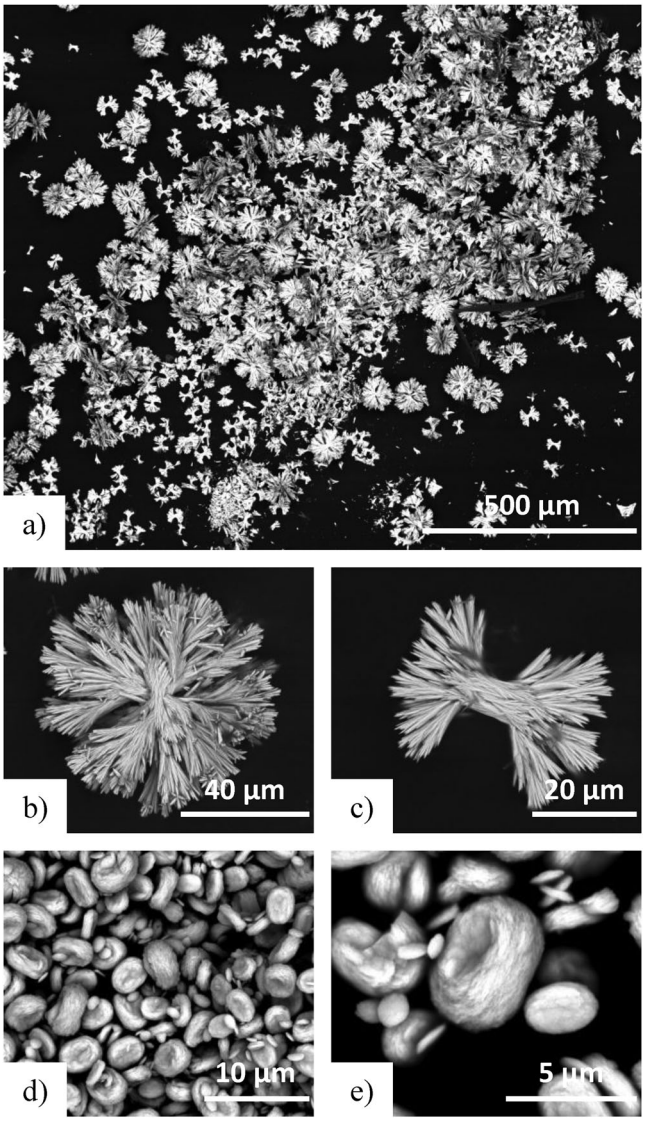


Figure 2. a)–e) Scanning electron microscope images of $PuCO_3OH(cr)$. a) to c) first synthesis, d) to e) second synthesis.

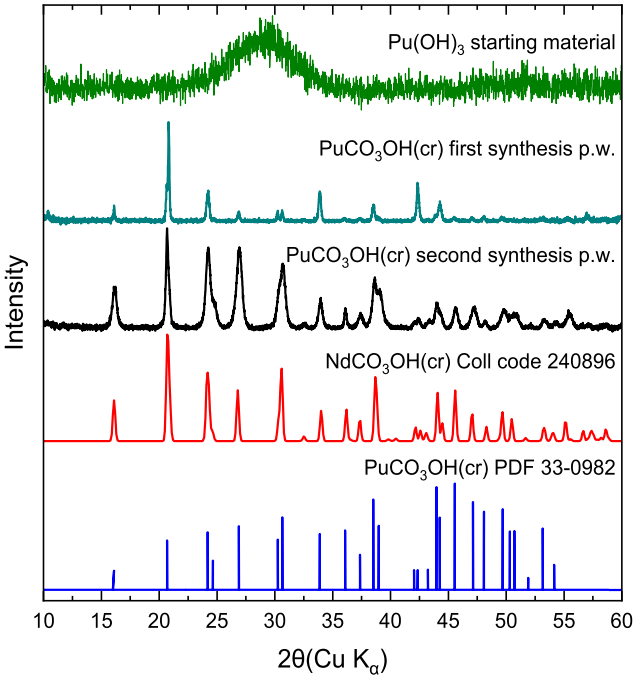


Figure 3. XRD patterns of the starting material $Pu(OH)_3$(am) (green), the transformation product $PuCO_3OH$(cr) (turquoise/black), and the references of previously reported $NdCO_3OH$(cr) (red)[33] and $PuCO_3OH$(cr) (blue).[31]

product, $PuCO_3OH$(cr), obtained in the present work in comparison to reference patterns for $NdCO_3OH$(cr)[33] and $PuCO_3OH$(cr).[31] In contrast to the X-ray amorphous $Pu(OH)_3$(am), the diffraction patterns of $PuCO_3OH$(cr) show sharp and well-defined peaks, corroborating its crystalline morphology. The excellent agreement with the diffraction patterns of orthorhombic $NdCO_3OH$(cr) and $PuCO_3OH$(cr) indicates that all three phases are isostructural.

From the results of VIS/NIR spectroscopy, SEM/EDX, and XRD, the transfromed Pu solid can unequivocally be identified as $PuCO_3OH$(cr).

Structural parameters for $PuCO_3OH$(cr) were derived from Rietveld analysis and Pu L3-edge EXAFS. Complementary to the refinement of the unit cell parameters based on powder XRD, EXAFS–as short range structural probe–provides additional details on the local Pu(III) coordination environment in $PuCO_3OH$(cr). Pu L3 EXAFS results are in accordance with the crystal structure obtained by Rietveld analysis and the isostructural $NdCO_3OH$(cr) system.

The experimental raw powder in XRD pattern was indexed on the orthorhombic unit cell (space group *Pnma, no. 5)* reported for $NdCO_3OH$(cr) by Feng 2007.[33] After replacing Nd by Pu in the Rietveld refinement, the unit cell parameters for $PuCO_3OH$(cr) were evaluated, see Table S2. The corresponding Rietveld Fit is shown in Figure S3. The Plutonium atom is coordinated by 8 O atoms from 5 carbonate groups (2 terminal and 3 bidentate) and 2 O atoms from 2 OH^-. The Pu—O bond lengths are between 2.35 to 2.76 Å and O—Pu—O bond angles range from 49.4° to 156.7°. Each C atom is coordinated by 3 O atoms with a bond length of (1.27–1.30) Å and O—C—O bond angles of (119.38–120.18)°. Each OH^- group bridges two plutonium atoms forming a $[Pu—O]_n$ chain. These chains are connected by carbonate groups and thus form a three-dimensional network. Figure 4 shows the elementary cell of $PuCO_3OH$(cr) along the spatial directions (a–d).

In addition to the analytical methods already mentioned $PuCO_3OH$(cr) was analyzed as dried material at the *KIT Light Source*. The EXAFS spectra of the Pu L3-edge and the corresponding R-space fits are shown in Figures 5 and 6.

Experimental EXAFS and Fourier transform are in good agreement with the corresponding fits. The latter used the crystal structure of $PuCO_3OH$(cr) determined by Rietveld analysis (see Figure 4).

Table 2 shows that two pure oxygen shells and two pure carbon shells were required to reproduce the EXAFS spectra. Pu—O2 is a combined shell of four different oxygen atoms with very similar Pu–O distances.

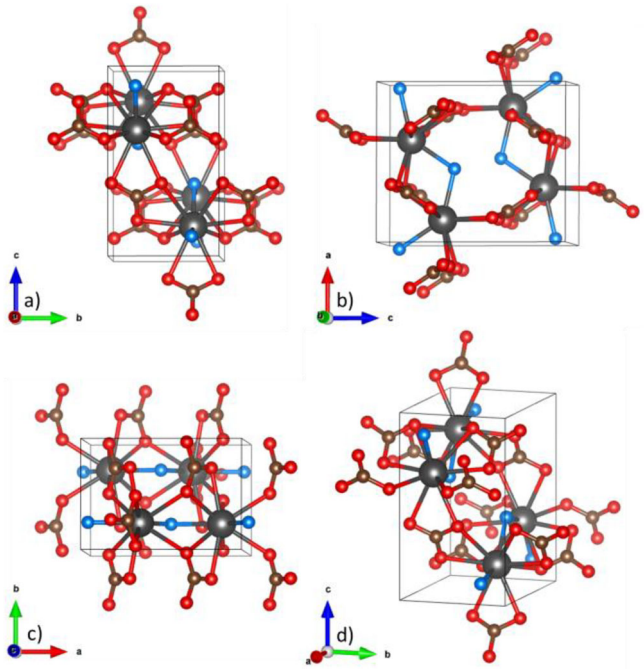


Figure 4. Solid-state structure of $PuCO_3OH(cr)$ looking into different axes (Pu, black; O from carbonate group, red; C, brown; O from OH, blue).

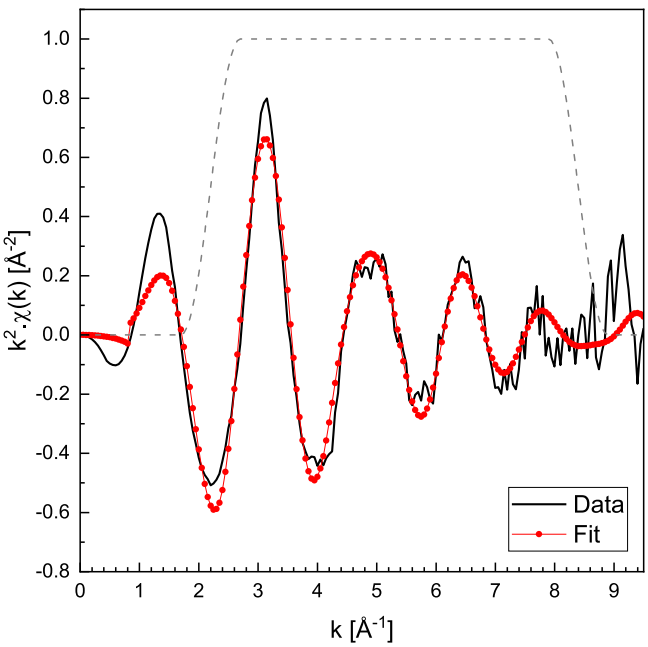


Figure 5. Pu L3-edge EXAFS spectra of $PuCO_3OH(cr)$, k^2-weighted $\chi(k)$ (black solid line) and corresponding fit (red line with filled circles). The fit range is indicated by dashed lines (grey).

Solubility Experiments and Thermodynamic Evaluation

The experimental molal solubility of $PuCO_3OH(cr)$ in carbonate containing 0.10 m NaCl solutions are displayed in Figure 7 as red solid diamonds. The data are provided in

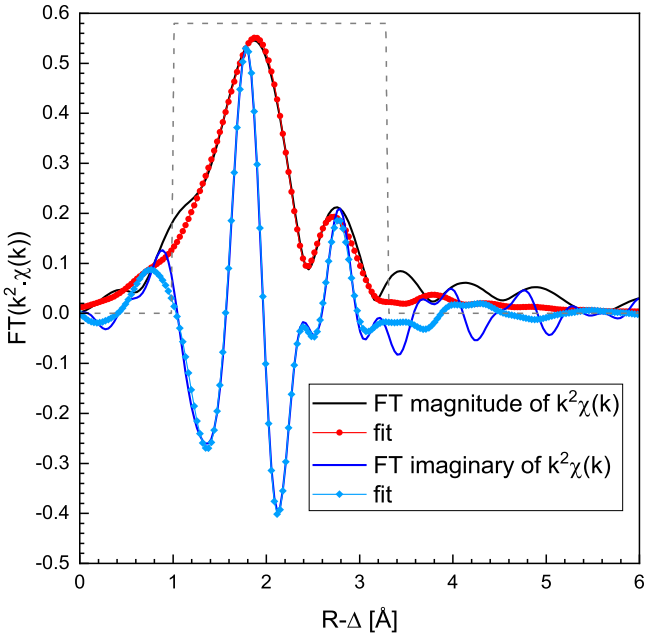


Figure 6. Fourier transform (FT) magnitude and imaginary part of k^2-weighted $\chi(k)$ (black and blue solid lines) and corresponding R-space fits (red and turquoise lines with filled circles). Window for forward FT is indicated by dashed lines (grey).

Table 2: Structural parameters obtained in this work from EXFAS evaluation of $PuCO_3OH(cr)$.[a)]

Sample	Path	CN	R [Å]	$\sigma 2$ [Å2]	ΔE_0 [eV]	R-factor [%]
$PuCO_3OH$	Pu-O1	2*	2.31	0.0096	2.7	0.7
	Pu-O2	8*	2.52	0.0139		
	Pu-C1	3*	2.94	0.0094		
	Pu-C2	2*	3.50	0.0015		

[a)] Fit errors: CN, ± 20%; $\sigma 2$, 0.0006 $Å^2$; R, 0.02 Å. * Held constant during the fit.

the (Table S5). The calculated model for $AnCO_3OH(cr)$ with An = Am/Cm based on the data from NEA-TDB[15] and the specific ion interaction theory (SIT),[34] and an updated model for Pu(III) derived in the present work are shown in Figure 7 as comparison. For the given experimental setup with pCO_2 fixed to 1%, the total carbonate concentration in the system systematically increases with pH_m. Consequently, pH_m values higher than ≈ 8.5 cannot be achieved in systems with I = 0.10 m without exceeding the intended ionic strength.

The samples were analyzed for pH_m and [Pu(III)] and overall showed good consistency. Between pH_m ≈ 5.5 and 7.0, the solubility of $PuCO_3OH(cr)$ systematically decreases by almost three orders of magnitude from log [Pu(III)] ≈ −5 to −8. The slope of the experimental curve is rather steep with m ≈ −3 to −2. For pH_m ≈ 7.0–8.0, the solubility reaches a minimum at log [Pu(III)] ≈ −8 and remains at a constant, quasi pH_m independent level. The observations can be explained by the solubility controlling equilibrium reactions. Under the experimental conditions, both hydrolysis

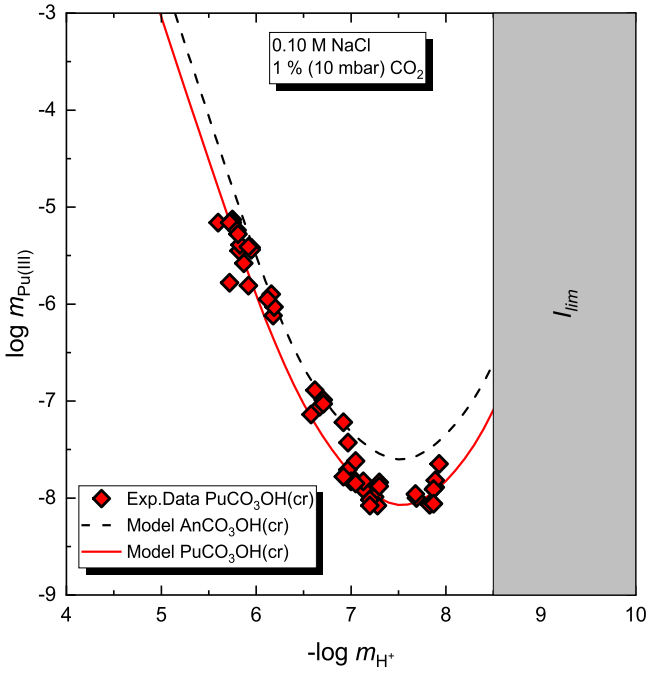


Figure 7. Experimental and calculated (SIT model) molal solubility of $PuCO_3OH$(cr) in 0.10 m NaCl under argon atmosphere with 1% (10 mbar) CO_2.

reactions and carbonate complexation of Pu^{3+} have to be considered.[15,29,35–41] The general expressions of the relevant equilibrium reactions in carbonate-containing NaCl solutions as well as the nomenclature of the stability constants used in the thermodynamic evaluation are summarized in Equations (1–4), where "*a*" and "*b*" are the stoichiometric numbers of H^+ and CO_3^{2-}, respectively.

I. Hydrolysis:

$$Pu^{3+} + aH_2O \Leftrightarrow Pu(OH)_a^{3-a} + aH^+ \quad (1)$$

$$\log^* \beta'_{a,0} = \log \left[Pu(OH)_a^{3-a}\right] + a \log [H^+] - \log \left[Pu^{3+}\right] \quad (1.1)$$

$$\log^* \beta^\circ_{a,0} = \log^* \beta'_{a,0} + \log \gamma_{Pu(OH)_a^{3-a}} + a \log \gamma_{H^+} - \log \gamma_{Pu^{3+}} - a \log a_w \quad (1.2)$$

with and

Solubility of $PuCO_3OH$(cr) regarding hydrolysis:

$$PuCO_3OH\,(cr) + (a-1)\,H_2O \Leftrightarrow Pu(OH)_a^{3-a} + CO_3^{2-} + (a-1)\,H^+ \quad (2)$$

with

$$\log^* K'_{s,a} = \log [Pu(OH)_a^{3-a}] + \log \left[CO_3^{2-}\right] + (a-1) \log [H^+] \quad (2.1)$$

and

$$\log^* K^\circ_{s,a} = \log^* K'_{s,a} + \log \gamma_{Pu(OH)_a^{3-a}} + \log \gamma_{CO_3^{2-}} \quad (2.2)$$

$$+ (a-1) \log \gamma_{H^+} - (a-1) \log a_w \quad (2.2)$$

2. Carbonate complexation:

$$Pu^{3+} + bCO_3^{2-} \Leftrightarrow Pu(CO_3)_b^{3-2b} \quad (3)$$

with

$$\log \beta'_{0,b} = \log \left[Pu(CO_3)_b^{3-2b}\right] - b \log \left[CO_3^{2-}\right] - \log \left[Pu^{3+}\right] \quad (3.1)$$

and

$$\log \beta^\circ_{0,b} = \log \beta'_{0,b} + \log \gamma_{Pu(CO_3)_b^{3-2b}} - b \log \gamma_{CO_3^{2-}} - \log \gamma_{Pu^{3+}} \quad (3.2)$$

Solubility of $PuCO_3OH$(cr) regarding carbonate complexation:

$$PuCO_3OH\,(cr) + (b-1)\,CO_3^{2-} + H^+ \Leftrightarrow Pu(CO_3)_b^{3-2b} + H_2O \quad (4)$$

with

$$\log^* K'_{s,b} = \log [Pu(OH)_b^{3-2b}] - (b-1) \log \left[CO_3^{2-}\right] - \log [H^+] \quad (4.1)$$

and

$$\log^* K^\circ_{s,b} = \log^* K'_{s,b} + \log \gamma_{Pu(OH)_b^{3-2b}} + \log a_w - (b-1) \log \gamma_{CO_3^{2-}} - \log \gamma_{H^+} \quad (4.2)$$

The number of reported thermodynamic constants for Pu(III) complexes with OH^- and CO_3^{2-} is rather limited. The 2020 compilation of the NEA-TDB lists indeed only data for the species $PuOH^{2+}$.[15] On the other hand, the interaction with hydroxide and carbonate has been well studied for trivalent Am and Cm by means of solubility experiments and time-resolved laser-induced fluorescence spectroscopy (TRLFS), and comprehensive chemical and thermodynamic models were developed.[15,28,29,39,40] Both, Am(III) and Cm(III) are considered highly reliable chemical analogs to model the behavior of Pu(III) based on the principle of oxidation state analogy.[29,42,43] In a first step, we have therefore compared our experimental solubility data for $PuCO_3OH$(cr) to the chemical–thermodynamic model reported by the NEA-TDB[15] for Am(III)/Cm(III) which is based on the specific ion interaction theory to account for ionic strength effects. It includes the solubility constant of $AmCO_3OH$(cr), the formation constants of $Am(OH)^{2+}$, $Am(OH)_2^+$, $Am(OH)_3$(aq), $Am(CO_3)^+$, $Am(CO_3)_2^-$, and $Am(CO_3)_3^{3-}$ and the corresponding ion interaction coefficients,[15,29] see Tables S3 and S4. Constants and parameters for the inactive carbonate system were taken from NEA-TDB as well. Innersphere An^{3+} and Cl^- complexes are negligble at $I = 0.10$ m and have not been included in the evaluation.[41,44,45]

The Am(III)/Cm(III) model displayed as dashed curve in Figure 7 describes the experimental solubility data for

Table 3: Selected thermodynamic data from NEA–TDB[15] and Neck.[29]

Species	$Log_{10}K^0$	Reaction
$Am(OH)^{2+}$	−7.200	$Am^{3+} + H_2O \rightleftharpoons AmOH^{2+} + H^+$
$Am(OH)_2^+$	−15.100	$Am^{3+} + 2H_2O \rightleftharpoons Am(OH)_2^+ + 2H^+$
$Am(OH)_3(aq)$	−26.200	$Am^{3+} + 3H_2O \rightleftharpoons Am(OH)_3(aq) + 3H^+$
$Am(CO_3)^+$	8.000	$Am^{3+} + CO_3^{2-} \rightleftharpoons AmCO_3^+$
$Am(CO_3)_2^-$	12.900	$Am^{3+} + 2CO_3^{2-} \rightleftharpoons Am(CO_3)_2^-$
$Am(CO_3)_3^{3-}$	15.000	$Am^{3+} + 3CO_3^{2-} \rightleftharpoons Am(CO_3)_3^{3-}$
$Pu(OH)^{2+}$	−6.180	$Pu^{3+} + H_2O \rightleftharpoons PuOH^{2+} + H^+$
$AmCO_3OH$ x0.5 H_2O(cr)	22.400	$Am^{3+} + CO_3^{2-} + 0.5H_2O(l) + OH^- \rightleftharpoons AmCO_3OH \times 0.5H_2O(cr)$
$AmCO_3OH$(cr)	−22.7	$AmCO_3OH \times xH_2O \rightleftharpoons Am^{3+}(aq) + OH^-(aq) + CO_3^{2-}(aq) + xH_2O(l)$
$Pu(OH)_3$(am)	14.58	$Pu(OH)_3(s)(am) + 3H^+ \rightleftharpoons Pu^{3+}(aq) + 3H_2O(l)$
$CO_2(aq)$	6.354	$H^+ + HCO_3^- \rightleftharpoons CO_2(aq) + H_2O(l)$
$CO_2(g)$	1.472	$CO_2(aq) \rightleftharpoons CO_2(g)$
HCO_3^-	10.329	$CO_3^{2-} + H^+ \rightleftharpoons HCO_3^-$

$PuCO_3OH$(cr) overall quite well. This concerns both the absolute Pu(III) concentration level as well as the shape of the curve which reflects the pH_m dependence. Still, the model slightly overestimates the experimental Pu(III) solubility level uniformly, i.e., over the entire pH_m range by about 0.4 log-units, suggesting that the solubility controlling $PuCO_3OH$(cr) solid phase is more stable than the Am(III) analog. By adjusting log $*K°_{s,0}$ from −8.4 (± 0.5)[15] (Neck:−8.7 (± 0.4)[29]) (Am value) to log $*K°_{s,0}$ = −8.84 (± 0.15), and replacing the hydrolysis constant log $*ß°_{1,0}$ for $AmOH_2^+$ by the reported value for the analog Pu species, a model for Pu(III) was evaluated. SIT ion-interaction coefficients and complexation constants log $\beta_{0,b}$ for the $An(CO_3)_b^{3-2b}$ species remained unchanged within the evaluation, see Table 3.

Speciation lines for the different Pu/Am(III) complexes calculated from the new Pu model are displayed in the (Figure S4). This plot reveals that the steep decrease in log [Pu(III)] at $pH_m \approx 5.5$–6.0 is particularly due to an equilibrium between $PuCO_3OH$(cr) and the Pu^{3+} aquo ion. Furthermore, the changing slope of the curve in the region around the solubility minimum at $pH_m \approx 7$–8 is related to the changing aqueous speciation where the Pu(III) carbonate complexes $PuCO_3^+$ and $Pu(CO_3)_2^-$ and the first hydrolysis species $PuOH^{2+}$ are predominant.

The results of the present study address relevant gaps in the field of fundamental research of Pu, and are at the same time of high relevance concerning the geochemical assessment of Pu chemistry in the context of nuclear waste disposal. In source term estimations performed within the safety assessment for nuclear waste repositories, implementation of solubility equilibria provides upper-limit concentrations for hazardous elements including radioactive isotopes. For Pu, two oxidation states are considered relevant under the conditions of a deep geological repository, namely Pu(III) and the sparingly soluble Pu(IV). The solubility of Pu(III) is often evaluated by assuming $Pu(OH)_3$(am) as the equilibrium solid phase.[12,13] This compound is the principal oxyhydroxide phase/precipitate of Pu(III) and holds rather high Pu(III) concentrations in near-neutral to slightly alkaline solutions. As direct evidence for the relevance of Pu(III)–carbonate

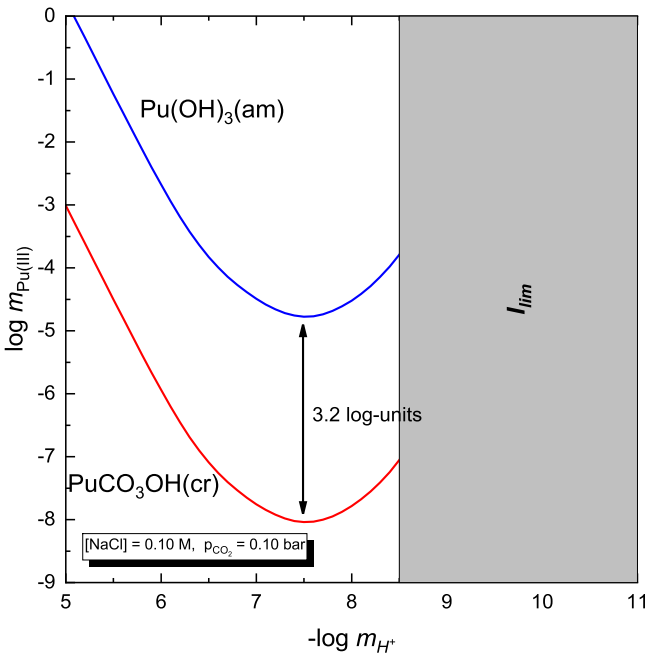


Figure 8. Calculated molal solubility (SIT model) of $PuCO_3OH$(cr) (red) and $Pu(OH)_3$(am) (blue) in 0.10 m NaCl with $pCO_2 = 0.01$ bar.

solid phases in aqueous solutions are lacking up to now, $Pu(OH)_3$(am) is considered for host rock systems and scenarios where carbonate is present. With the solubility constantly derived in this work for $PuCO_3OH$(cr), the picture changes substantially. Figure 8 compares the calculated solubility of $Pu(OH)_3$(am)[15] and $PuCO_3OH$(cr) for solutions with 0.10 M NaCl and $pCO_2 = 0.01$ bar. For $pH_m \leq 8.5$, the solubility of $PuCO_3OH$(cr) is about 3.2 orders of magnitude lower than that of $Pu(OH)_3$(am). At pH_m 7.5 the concentration of Pu(III) approaches ≈ −8, i.e., a level that is close to that of the notorious quasi insoluble Pu(IV) with log [Pu(IV)] ≈ −7.9 (total Pu(IV) including contributions from Pu(IV) colloids[46]). The fact that $PuCO_3OH$(cr) forms spontaneously and in situ from the precursor $Pu(OH)_3$(am) in presence of carbonate

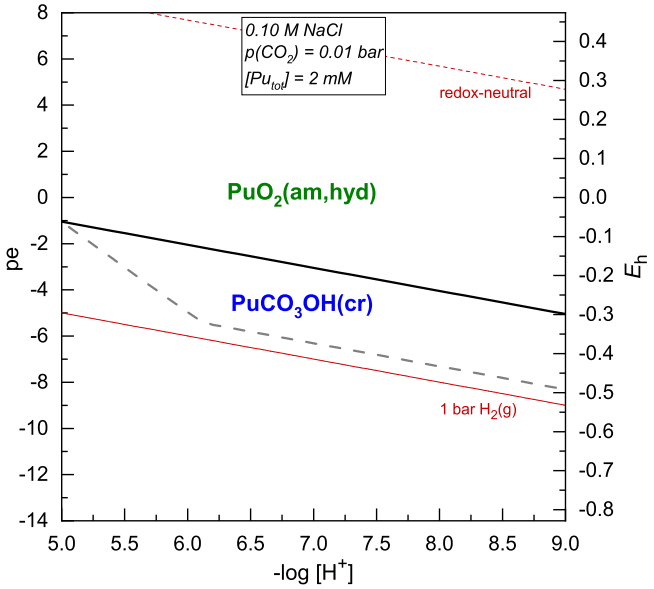


Figure 9. Pu Pourbaix diagram calculated for $[Pu_{tot}] = 2$ mM in 0.10 M NaCl solution in presence of carbonate $pCO_2 = 0.01$ bar. The grey dashed line indicates Pu(III)–Pu(IV) transition borderline in the absence of carbonate.

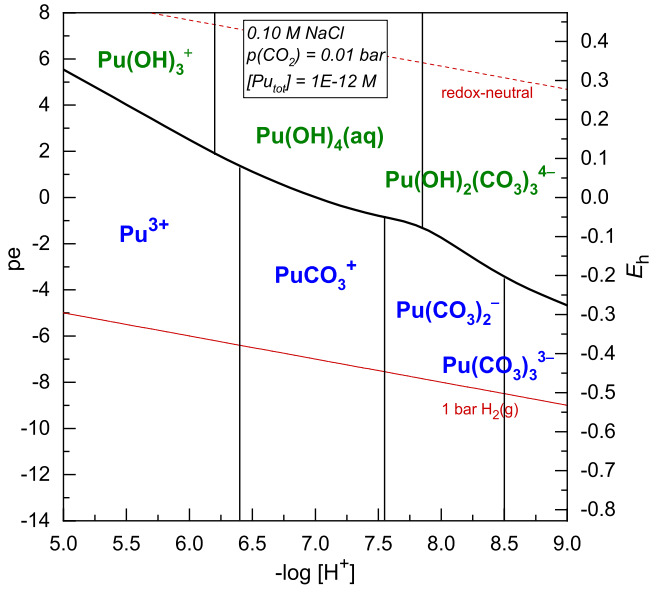


Figure 10. Pu Pourbaix diagram for aqueous Pu species calculated for $[Pu_{tot}] = 1{\cdot}10^{-12}$ M in 0.10 M NaCl solution in presence of carbonate $pCO_2 = 0.01$ bar.

makes $PuCO_3OH(cr)$ a realistic and highly relevant compound in geochemical model calculations, representing a potential sink for dissolved Pu(III) that dramatically reduces its concentration in solution. Note, that the overall pH_m dependencies of both solid phases and their solubility curves is identical for the system with constant pCO_2 displayed in Figure 8 (the formal replacement of two OH^- ligands in $Pu(OH)_3(am)$ by one CO_3^{2-} to build $PuCO_3OH(cr)$ leads to the same pH/OH^- demands as the equilibrium concentration log $[CO_3^{2-}]$ defined by $CO_2(g) + H_2O = CO_3^{2-} + 2H^+$ increases by a factor 2 per pH_m unit). The specified ionic strength is $I = 0.10$ m. This means pH values greater than 8.5 are not possible. This is because the increasing carbonate concentration would exceed the specified ionic strength. This change in a system with fixed total carbonate concentration, e.g., $[C_{tot}] = 2$ mM–a level typically found in pH near-neutral systems where the total carbonate is limited by calcite (Figure S5).

As $PuCO_3OH(cr)$ is significantly more stable/less soluble than $Pu(OH)_3(am)$, it will control the Pu(III) solubility once sufficient carbonate is present in a Pu system, leading to substantial changes in the position of the Pu(III)–Pu(IV) redox borderline. The Pu Pourbaix diagram in Figure 9 highlights the result for the model case $[Pu_{tot}] = 2$ mM in 0.1 m NaCl with $pCO_2 = 0.01$ bar, where the Pu(III)/Pu(IV) borderline shifts by up to 3.3 pe-units to higher values compared to the carbonate free system indicated by the grey dashed line. For the same model case, the changes in the aqueous Pu(III) and Pu(IV) speciation due to formation of Pu–CO_3 complexes leads to a net stabilization of the Pu(III) oxidation state and a shift of the corresponding Pu(III)(aq)–Pu(IV)(aq) borderline by up to 2 pe-units to more positive pe values, see Figure 10, compared to the pure hydrolysis system (Figure S1).[21]

Conclusions

We report the first ever systematic solubility study on $PuCO_3OH(cr)$, an important Pu(III) solid phase in the context of nuclear waste disposal, and presents a comprehensive chemical and thermodynamic model to describe Pu(III) solubility and speciation in aquatic carbonate containing NaCl solutions.

The $PuCO_3OH(cr)$ solid phase was successfully synthesized from $Pu(OH)_3(am)$ in aqueous solution with trace concentrations of carbonate at 23 ± 2 °C. It was characterized by VIS/NIR, SEM/EDX, and powder XRD. The crystal structure of $PuCO_3OH(cr)$ was determined by using Rietveld analysis and visualized with VESTA program. The Pu L3 edge EXAFS of $PuCO_3OH(cr)$ was investigated at the *KIT Light source* and the experimental EXAFS and Fourier transform of the L3 edge was successfully reproduced using 2 pure oxygen shells and 2 pure carbon shells. In a glove box with argon atmosphere and 10 mbar CO_2 partial pressure, batch solubility experiments were performed in 0.10 m NaCl solutions (pH range 5.5–8.0). The experimental solubility data fit excellently to calculated solubilities of a new $AnCO_3OH(cr)$ SIT model. The thermodynamic solubility constant $\log{}^*K^\circ_{s,0} = -8.84$ (± 0.15) was calculated from the experimental solubility data. The comparison of the calculated solubilities of $PuCO_3OH(cr)$ and $Pu(OH)_3(am)$ under repository-relevant conditions shows a significantly lower solubility of $PuCO_3OH(cr)$ in a pH range of 4.5–10.0. Under neutral pH conditions, the difference is up to 3 orders of magnitude. The latter and the fact that $PuCO_3OH(cr)$ spontaneous forms from $Pu(OH)_3(am)$ in solutions with trace levels of carbonate show that it can be realistically considered for geochemical model calculations and source-term estimations. In conclusion, traces of carbonate reduce

the mobility and solubility of trivalent plutonium due to the formation of a sparingly soluble carbonate containing solid phase.

Acknowledgements

The authors acknowledge the KIT Light Source for the provision of beamtime at the INE-Beamline operated by the Institute for Nuclear Waste Disposal (KIT-INE) and authors would like to thank the Institute for Beam Physics and Technology (KIT-IBPT) for the operation of the storage ring (Karlsruhe Research Accelerator, KARA).

Conflict of Interests

The authors declare no conflict of interest.

Data Availability Statement

The data that support the findings of this study are available in the supplementary material of this article.

Keywords: Carbonate complexation · Plutonium · Pu L3-edge EXAFS · Pu(III)-hydroxocarbonate · Solubility

[1] H. Geckeis, M. Zavarin, B. Salbu, O. C. Lind, L. Skipperud, in *Plutonium Handbook*, 2nd ed. (Eds.: D. L. Clark, D. A. Geeson, R. J. Hanrahan), American Nuclear Society, Washington, DC **2019**.

[2] H. Geckeis, K. J. Röhlig, K. Mengel, *Chemie in unserer Zeit* **2012**, *46*, 282–293, https://doi.org/10.1002/ciuz.201200583.

[3] M. Altmaier, X. Gaona, T. Fanghänel, *Chem. Rev.* Washington, DC **2013**, *113*, 901–943, https://doi.org/10.1021/cr300379w.

[4] H. Wanner, *Pure Appl. Chem.* **2007**, *79*, 875–882, https://doi.org/10.1351/pac200779050875.

[5] V. Metz, H. Geckeis, E. González-Robles, A. Loida, C. Bube, B. Kienzler, *Radiochim. Acta* **2012**, *100*, 699–713, https://doi.org/10.1524/ract.2012.1967.

[6] G. R. Choppin, *Radiochim. Acta* **2003**, *91*, 645–650, https://doi.org/10.1524/ract.91.11.645.23469.

[7] R. J. Silva, H. Nitsche, *Radiochim. Acta* **1995**, *70-71*, 377–396, https://doi.org/10.1524/ract.1995.7071.s1.377.

[8] E. Gaucher, C. Robelin, J. M. Matray, G. Ngérel, Y. Gros, J. F. Heitz, A. Vinsot, H. Rebours, A. Cassagnabère, A. Bouchet, *Phys. Chem. Earth* **2004**, *29*, 55–77, https://doi.org/10.1016/j.pce.2003.11.006.

[9] M. Altmaier, H. Geckeis, *Actinide Research Quarterly* published by Los Alamos National Laboratory, Los Alamos, USA.

[10] K. Maher, J. R. Bargar, G. E. Brown Jr, *Inorg. Chem.* **2013**, *52*, 3510–3532, https://doi.org/10.1021/ic301686d.

[11] N. M. Edelstein, J. Fuger, J. J. Katz, L. R. Morss, in *The Chemistry of the Actinide and Transactinide Elements* (Eds.: L. R. Morss, N. M. Edelstein, J. Fuger), Springer, Dordrecht, **2006**, pp. 1753–1835, https://doi.org/10.1007/1-4020-3598-5.

[12] U. Berner, Solubility of Radionuclides in a Bentonite Environment for Provisional Safety Analyses for SGT-E2, Nagra Technical Report, **2014**.

[13] U. Berner, Solubility of Radionuclides in a Concrete Environment for Provisional Safety Analyses for SGT-E2, Nagra Technical Report, **2014**.

[14] M. Altmaier, X. Gaona, D. Fellhauer, D. L. Clark, W. Runde, D. E. Hobart, in *Plutonium Handbook*, 2nd ed. (Eds.: D. L. Clark, D. A. Geeson, R. J. Hanrahan), American Nuclear Society, **2019**.

[15] I. Grenthe, X. Gaona, L. Rao, A. Plyasunov, W. Runde, B. Grambow, R. Konings, A. Smith, E. Moore, in *Chemical Thermodynamics*, Vol. *14*, OECD Nuclear Energy Agency (NEA), Boulogne-Billancourt (France) **2020**.

[16] A. Tasi, X. Gaona, D. Fellhauer, M. Böttle, J. Rothe, K. Dardenne, D. Schild, M. Grivé, E. Colàs, J. Bruno, K. Källström, M. Altmaier, H. Geckeis, *Radiochim. Acta* **2018**, *106*, 259–279, https://doi.org/10.1515/ract-2017-2870.

[17] V. Neck, M. Altmaier, T. Fanghänel, *C. R. Chim.* **2007**, *10*, 959–977, https://doi.org/10.1016/j.crci.2007.02.011.

[18] W. Stumm, J. J. Morgan, *Aquatic Chemistry: Chemical Equilibria and Rates in Natural Waters*, 3 ed., John Wiley & Sons, New York, **2013**.

[19] W. Runde, *Los Alamos Science* **2000**, *2*, 392–411.

[20] J. I. Kim, C. Lierse, F. Baumgartner, in *Plutonium Chemistry 216* (Eds.: W. T. Carnall, G. R. Choppin), ACS Publications, Washington, DC **1983**.

[21] J. Schepperle, Dissertation thesis, Karlsruher Institut für Technologie (Karlsruhe), **2020**.

[22] T. Kobayashi, D. Fellhauer, T. Sasaki, *J. Solution Chem.* **2021**, *50*, 443–457, https://doi.org/10.1007/s10953-021-01080-9.

[23] H. Nitsche, R. Silva, *Radiochim. Acta* **1996**, *72*, 65–72, https://doi.org/10.1524/ract.1996.72.2.65.

[24] T. Yamaguchi, Y. Sakamoto, T. Ohnuki, *Radiochim. Acta* **1994**, *66-67*, 9–14, https://doi.org/10.1524/ract.1994.6667.s1.9.

[25] R. Guillaumont, T. Fanghänel, J. Fuger, I. Grenthe, V. Neck, D. A. Palmer, M. H. Rand, *Update on the Chemical Thermodynamics of Uranium, Neptunium, Plutonium, Americium and Technetium, Vol. 5*, OECD Nuclear Energy Agency, Issy-les-Moulineaux, France, **2003**.

[26] M. L. Salutsky, L. L. Quill, *J. Am. Chem. Soc.* **1950**, *72*, 3306–3307, https://doi.org/10.1021/ja01163a537.

[27] R. L. N. Sastry, S. R. Yoganarasimhan, P. N. Mehrotra, C. N. R. Rao, *Journal of Inorganic and Nuclear Chemistry* **1966**, *28*, 1165–1177, https://doi.org/10.1016/0022-1902(66)80442-6.

[28] W. Runde, G. Meinrath, J. I. Kim, *Radiochim. Acta* **1992**, *58-59*, 93–100, https://doi.org/10.1524/ract.1992.5859.1.93.

[29] V. Neck, T. Fanghänel, J. I. Kim, Forschungszentrum Karlsruhe GmbH, **1998**.

[30] A. R. Felmy, D. Rai, R. W. Fulton, *Radiochim. Acta* **1990**, *50*, 193–204, https://doi.org/10.1524/ract.1990.50.4.193.

[31] P. Hagan, J. Navratil, R. Cichorz, *J. Inorg. Nucl. Chem.* **1981**, *43*.

[32] D. Cohen, *J. Inorg. Nucl. Chem.* **1961**, *18*, 211–218, https://doi.org/10.1016/0022-1902(61)80390-4.

[33] W.-J. Feng, G.-P. Zhou, Z.-B. Liu, Y. Xu, *Acta Crystallogr. E: Struct. Rep. Online* **2007**, *63*, i174–i174, https://doi.org/10.1107/S160053680703721X.

[34] L. Ciavatta, *Ann. Chim.(Rome)* **1980**, *70*, 551.

[35] T. Fanghänel, T. Könnecke, H. Weger, P. Paviet-Hartmann, V. Neck, J. I. Kim, *J. Solution Chem.* **1999**, *28*, 447–462. https://doi.org/10.1023/A:1022664013648.

[36] H. Nitsche, E. M. Standifer, *Radiochim. Acta* **1989**, *46*, 185–190, https://doi.org/10.1524/ract.1989.46.4.185.
[37] S. Stadler, J. I. Kim, *Radiochim. Acta* **1988**, *44-45*, 39–44, https://doi.org/10.1524/ract.1988.4445.1.39.
[38] T. Fanghänel, H. T. Weger, T. Könnecke, V. Neck, P. Paviet-Hartmann, E. Steinle, J. I. Kim, *Radiochim. Acta* **1998**, *82*, 47–54, https://doi.org/10.1524/ract.1998.82.special-issue.47.
[39] W. Runde, Dissertation thesis, Technische Universität München (München), **1993**.
[40] W. Runde, Diplomarbeit thesis, Technische Universität München (München), **1990**.
[41] V. Neck, M. Altmaier, T. Rabung, J. Lützenkirchen, T. Fanghänel, *Pure Appl. Chem.* **2009**, *81*, 1555–1568, https://doi.org/10.1351/PAC-CON-08-09-05.
[42] T. Fanghänel, V. Neck, *Pure Appl. Chem.* **2002**, *74*, 1895–1907, https://doi.org/10.1351/pac200274101895.
[43] G. R. Choppin, *Radiochim. Acta* **1983**, *32*, 43–54, https://doi.org/10.1524/ract.1983.32.13.43.
[44] T. Könnecke, T. Fanghänel, J. Kim, *Radiochim. Acta* **1997**, *76*, 131–136.
[45] T. Fanghänel, J. I. Kim, R. Klenze, Y. Kato, *J. Alloys Compd.* **1995**, *225*, 308–311, https://doi.org/10.1016/0925-8388(94)07131-4.
[46] M. Altmaier, V. Neck, T. Fanghänel, *Radiochim. Acta* **2004**, *92*, 537–543, https://doi.org/10.1524/ract.92.9.537.54983.
[47] V. Münchow, R. Steudel, *Zeitschrift für anorganische und allgemeine Chemie* **1994**, *620*, 121–126.
[48] M. Altmaier, V. Neck, T. Fanghänel, *Radiochim. Acta* **2008**, *96*, 541–550, https://doi.org/10.1524/ract.2008.1535.
[49] A. Baumann, E. Yalçıntaş, X. Gaona, M. Altmaier, H. Geckeis, *New J. Chem.* **2017**, *41*, 9077–9086, https://doi.org/10.1039/C7NJ01816A.
[50] M. Altmaier, V. Metz, V. Neck, R. Müller, T. Fanghänel, *Geochim. Cosmochim. Acta* **2003**, *67*, 3595–3601, https://doi.org/10.1016/S0016-7037(03)00165-0.